POLISH POLAR RESEARCH
vol. 29, no. 4, pp. xxx–xxx, 2008

3D seismic model of the uppermost crust of the Admiralty Bay area, King George Island, West Antarctica

Mariusz MAJDAŃSKI [1], Piotr ŚRODA [1], Michał MALINOWSKI [1], Wojciech CZUBA[1], Marek GRAD [2,1], Aleksander GUTERCH [1] and Endre HEGEDŰS [3]

[1] *Instytut Geofizyki, Polskiej Akademii Nauk, Księcia Janusza 64, 01-452 Warszawa, Poland*
<mmajd@igf.fuw.edu.pl> <psroda@igf.edu.pl> <michalm@igf.edu.pl> <wojt@igf.edu.pl>
<aguterch@igf.edu.pl>

[2] *Instytut Geofizyki, Uniwersytet Warszawski, Pasteura 7, 02-093 Warszawa, Poland*
<mgrad@mimuw.edu.pl>

[3] *Eötvös Loránd Geophysical Institute of Hungary, Kolumbusz utca 17-23,*
Budapest H-1145, Hungary <hegedus@elgi.hu>

Abstract: The understanding of the evolution of Antarctica is one of the main challenges in Earth sciences and the structure of its crust is a key to investigate the tectonic processes. One of the most interesting areas of the West Antarctica is the transition from the oceanic crust of the Pacific Plate to the continental crust of the Antarctic Peninsula through the South Shetland Trench and the volcanic arc of the South Shetland Islands toward the Bransfield Strait rift. In 2007, a 3D seismic survey was performed in the Admiralty Bay (King George Island, South Shetland Islands). It targeted the shallow crustal structure of the volcanic arc. The air-gun shots were recorded using 47 seismic land stations in two deployments. Good quality data allowed for 3D tomographic modelling of the study area. Sonar measurements data were used to generate the bathymetry. The first-arrival travel times were inverted for the P-wave velocity models using two different methods: "smooth" seismic tomography with the use of the Iterative Back Projection code (IBP) and tomography with layers (JIVE3D). Obtained velocity anomalies are correlated with the fault structures determined from surface mapping. We were able to trace the Ezcurra Fault down to the depth of 2 km and to recognize the velocities related to the Barton Horst (4.5 km/s) and the Warszawa and Kraków blocks (3.5 km/s). The Mackellar Fault can not be recognized in the deeper part of our model. The estimation of the model uncertainty indicates that the inferred fault structures are resolvable by our dataset.

Key words: Antarctica, King George Island, seismic tomography, crustal structure, wide angle experiment.

Tectonic framework

The South Shetland Islands were separated from the Antarctic Peninsula in the Tertiary (Dalziel and Elliot 1973). The Drake Passage and Western Scotia Sea were

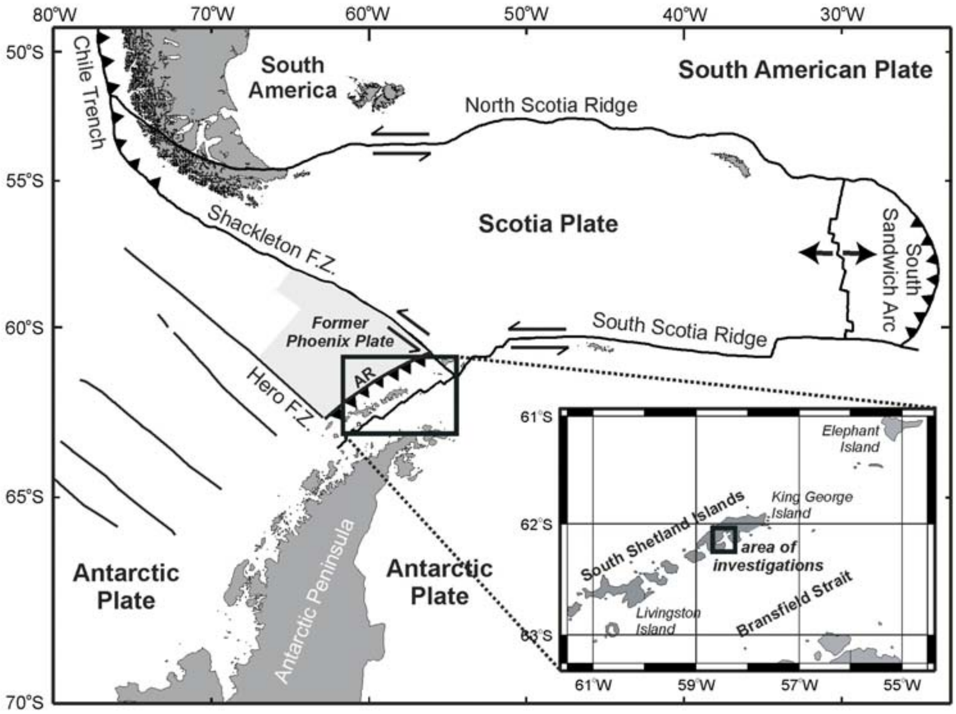

Fig. 1. The King George Island is a part of the South Shetland Islands archipelago located in the West Antarctica (map after Taylor *et al.* 2008). This tectonically active area is located in the contact zone of the Scotia Plate and the Antarctic Plate. It is a part of the Cenozoic subduction system that includes Meso/Cenozoic intrusions of volcanic rocks connected to rifting processes in the Bransfield Strait. Localization of the area of investigation in the Admiralty Bay is marked with a frame in the insert. AR – Aluk Ridge.

opened at the same time when the North and South Scotia Ridges were separated from the southern part of South America (Acosta *et al.* 1992). This area is characterised by a complicated subduction history and its schematic tectonic map is presented in Fig. 1. The western margin of the Antarctica between the Shackleton Fracture Zone and the Hero Fracture Zone and the Aluk Ridge was a convergent margin during the last 21 Ma. This subduction was countervailed by the generation of a new oceanic crust in the western Drake Passage. The subduction has stopped about 4 Ma ago and there is no observed activity at present (Barker 1982; Barker and Dalziel 1983). The Bransfield Rift, and the Bransfield Platform represent a back-arc basin of the South Shetland Islands volcanic arc active in the late Mesozoic–Cenozoic. The initiation of the Bransfield Basin is dated at the late Oligocene–Early Miocene (Birkenmajer 1989). In the late Cenozoic a tensional regime generated a 40 km wide rift in the Bransfield Strait which separates the Bransfield Platform and the South Shetland Islands Microplate (Gonzalez-Ferran 1985). The crustal structure of the Bransfield Trough and the South Shetland Island has been studied using deep seis-

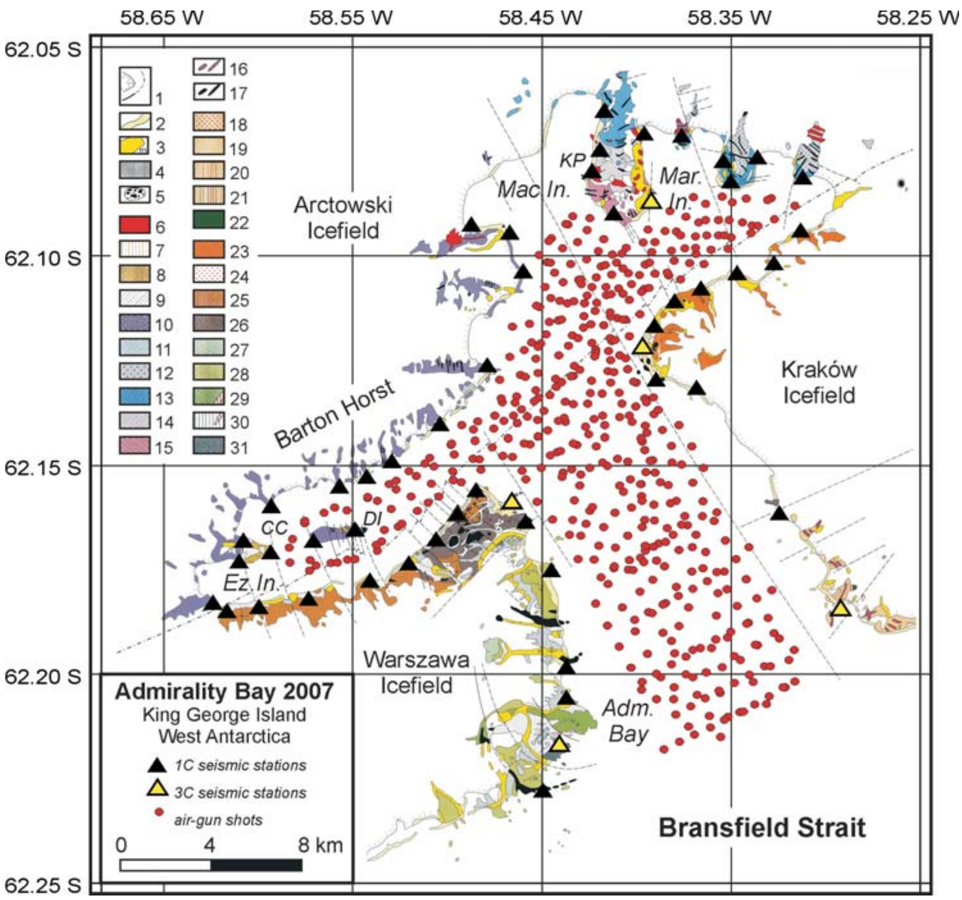

Fig. 2. The geological map of the Admiralty Bay (after Birkenmajer 2003) with marked geometry of the experiment: red dots – air gun shots, triangles – stations localization (black – 1C Texan station, yellow – 3C Hungarian station). The main faults: Ezcurra and Mackellar divide the area into three blocks: Barton Horst to the north, Warszawa and Kraków blocks to the south. Ez. In. – Ezcurra Inlet; CC – Cordozo Cove; DI – Dufayel Island; Mac In. – Mackellar Inlet; KP – Keller Peninsula; Mar. In. – Martel Inlet; Adm. Bay – Admiralty Bay. The geological details (marked with numbers 1–31) as in Birkenmajer 2003.

mic sounding that revealed its complicated structure (Guterch *et al.* 1985, 1998; Birkenmajer and Keller 1990; Środa 1991, 2002; Środa *et al.* 1997; Grad *et al.* 1992, 1993, 2002; Janik *et al.* 2003; Christeson *et al.* 2003). Teleseismic observations shows NW-SE tension and remarks of the rifting (Pelayo and Wiens 1989). Our experiment focused on the area of the Admiralty Bay, King George Island, South Shetland Islands. This area forms a contact zone of the three tectonic blocks: Barton Horst, Warszawa block and Kraków block. These blocks are separated by several faults known from surface geology (Birkenmajer 2003). The main goal was to delineate these faults in depth, especially the SW-NE trending Ezcurra Fault and the

Table 1

Coordinates of all stations in two deployments of the experiment. Some of the stations were deployed almost in the same place, while some were moved to different localization. The three component stations (HUN1-HUN5) were operating in the same place during the whole experiment

Deployment 1			Deployment 2			Deployment 1			Deployment 2		
Name	Long W [deg]	Lat S [deg]	Name	Long W [deg]	Lat S [deg]	Name	Long W [deg]	Lat S [deg]	Name	Long W [deg]	Lat S [deg]
TX1A	62.22734	58.44949	**–**	–	–	**TX28A**	62.07920	58.42370	**TX28B**	62.07920	58.42370
TX2A	62.20518	58.43715	**–**	–	–	**TX29A**	62.08942	58.41202	**TX29B**	62.08942	58.41202
TX3A	62.19779	58.43717	**–**	–	–	**TX30A**	62.07026	58.39595	**TX30B**	62.06973	58.39575
TX4A	62.17467	58.44514	**–**	–	–	**TX31A**	62.07088	58.37614	**TX31B**	62.07088	58.37614
TX5A	62.15547	58.48491	**TX5B**	62.15549	58.48488	**TX32A**	62.07680	58.35403	**TX32B**	62.07661	58.35397
TX6A	62.16108	58.49465	**TX6B**	62.16097	58.49488	**TX33A**	62.08177	58.35024	**TX33B**	62.08174	58.35006
TX7A	62.16727	58.50605	**TX7B**	62.16719	58.50613	**TX34A**	62.07600	58.33597	**TX34B**	62.07580	58.33617
TX8A	62.17303	58.52050	**TX8B**	62.17297	58.52047	**TX35A**	62.08084	58.31205	**TX35B**	62.08086	58.31234
TX9A	62.17716	58.54095	**TX9B**	62.17711	58.54090	**TX36A**	62.09350	58.31319	**TX36B**	62.09347	58.31438
TX10A	62.18152	58.57352	**TX10B**	62.18152	58.57352	**TX37A**	62.10131	58.32725	**TX37B**	62.10103	58.32715
TX11A	62.18340	58.59960	**TX11B**	62.18337	58.60007	**TX38A**	62.10365	58.34690	**TX38B**	62.10363	58.34726
TX12A	62.18451	58.61653	**TX12B**	62.18446	58.61698	**TX39A**	62.10731	58.36613	**TX39B**	62.10728	58.36614
TX13A	62.18236	58.62409	**–**	–	–	**–**	–	–	**TX40B**	62.11045	58.37976
–	–	–	**TX14B**	62.17260	58.61003	**TX41A**	62.11630	58.39054	**TX41B**	62.11640	58.39098
TX15A	62.17043	58.59355	**TX15B**	62.17046	58.59349	**TX42A**	62.12914	58.38979	**TX42B**	62.12860	58.38976
TX16A	62.16747	58.60775	**TX16B**	62.16759	58.60743	**TX43A**	62.13112	58.36823	**–**	–	–
TX17A	62.15926	58.59319	**TX17B**	62.15926	58.59319	**TX44A**	62.16106	58.32457	**–**	–	–
TX18A	62.16763	58.57078	**TX18B**	62.16754	58.57081	**–**	–	–	**TX46B**	62.16309	58.45867
TX19A	62.16492	58.54887	**TX19B**	62.16460	58.54916	**–**	–	–	**TX47B**	62.12123	58.39666
TX20A	62.15458	58.55716	**TX20B**	62.15466	58.55627	**–**	–	–	**TX48B**	62.10318	58.45999
TX21A	62.14850	58.52954	**TX21B**	62.14850	58.52954	**–**	–	–	**TX49B**	62.15227	58.54260
TX22A	62.13986	58.50399	**TX22B**	62.13986	58.50399	**HUN1**	62.158200	58.465810	**HUN1**	62.15820	58.46581
TX23A	62.12577	58.47891	**–**	–	–	**HUN2**	62.216270	58.440700	**HUN2**	62.21627	58.44070
TX24A	62.09396	58.46708	**TX24B**	62.09396	58.46708	**HUN3**	62.183740	58.292170	**HUN3**	62.18374	58.29217
TX25A	62.09199	58.48739	**TX25B**	62.09199	58.48739	**HUN4**	62.121230	58.396660	**HUN4**	62.12123	58.39666
TX26A	62.06480	58.41698	**TX26B**	62.06480	58.41698	**HUN5**	62.086430	58.392350	**HUN5**	62.08643	58.39235
TX27A	62.07415	58.41947	**TX27B**	62.07415	58.41947						

NW-SE trending Mackellar Fault and to recognize the differences of the blocks in the uppermost structure of the crust.

Data acquisition and seismic wave field

The experiment was done in February 2007, and its geometry is presented in Fig. 2. A total number of 47 seismic stations were located on the coast of the Ad-

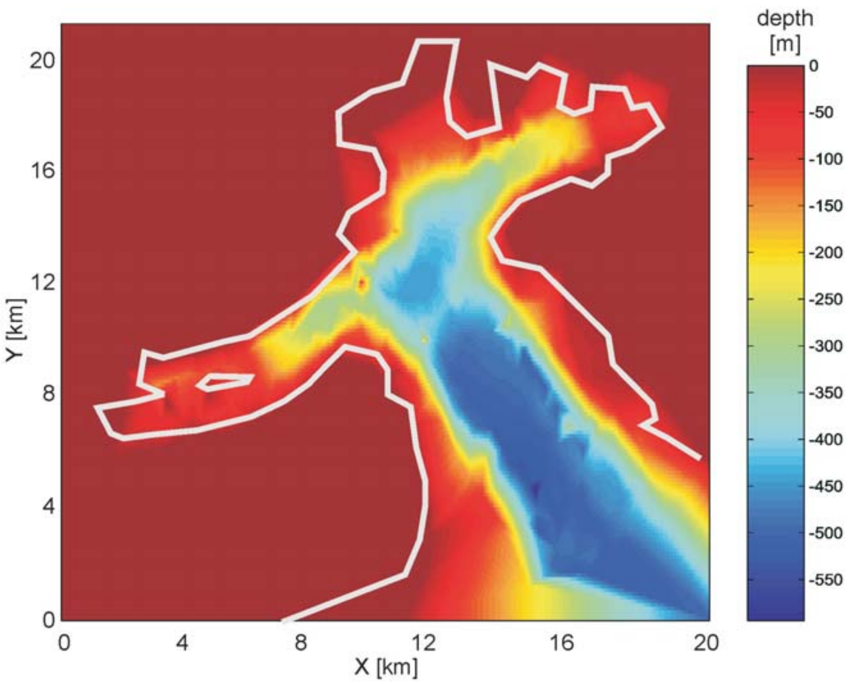

Fig. 3. The estimated shape of the sea floor. For each shot point the depth to the sea floor was measured by the ship echosounder. All measurements with additional points for stations (with the depth value of 0 m) were used to interpolate the shape of the sea floor. The result of bicubic spline interpolation is presented in the colour scale. The coast line is marked with white line.

miralty Bay, Ezcurra Inlet, Mackellar Inlet and Martel Inlet in two deployments. 42 one-component (1C) Reftek 125 "Texan" stations with 4.5 Hz geophones were recovered after the first part of the experiment to secure the data and to replace the batteries. The original power supply of the Reftek 125 was not sufficient in Antarctic conditions, therefore additional external battery packs were used. In the second deployment some of the stations were installed in different sites (see Table 1 for details) to improve the ray coverage of the experiment. The position of each station location was determined by GPS. We used also five three-component (3C) Hungarian stations (constructed at Eötvös Loránd Geophysical Institute in Budapest – ELGI) with 1 Hz Mark4 geophones that were recording continuously during the whole experiment. Two air-guns with the total capacity of 40 dm^3 were used as seismic sources. The seismic waves were generated along 21 profiles with a shot spacing of 0.7 km (every 4 minutes in average). Spacing between the profiles was about 1 km. The effect of the water depth on the observed travel times is significant, therefore it was necessary to include the bathymetry in our model. During the experiment we used an echosounder to measure the depth to the sea bottom beneath each shot. A total number of 449 values for shots and 52 localizations of stations with zero depth were used to cre-

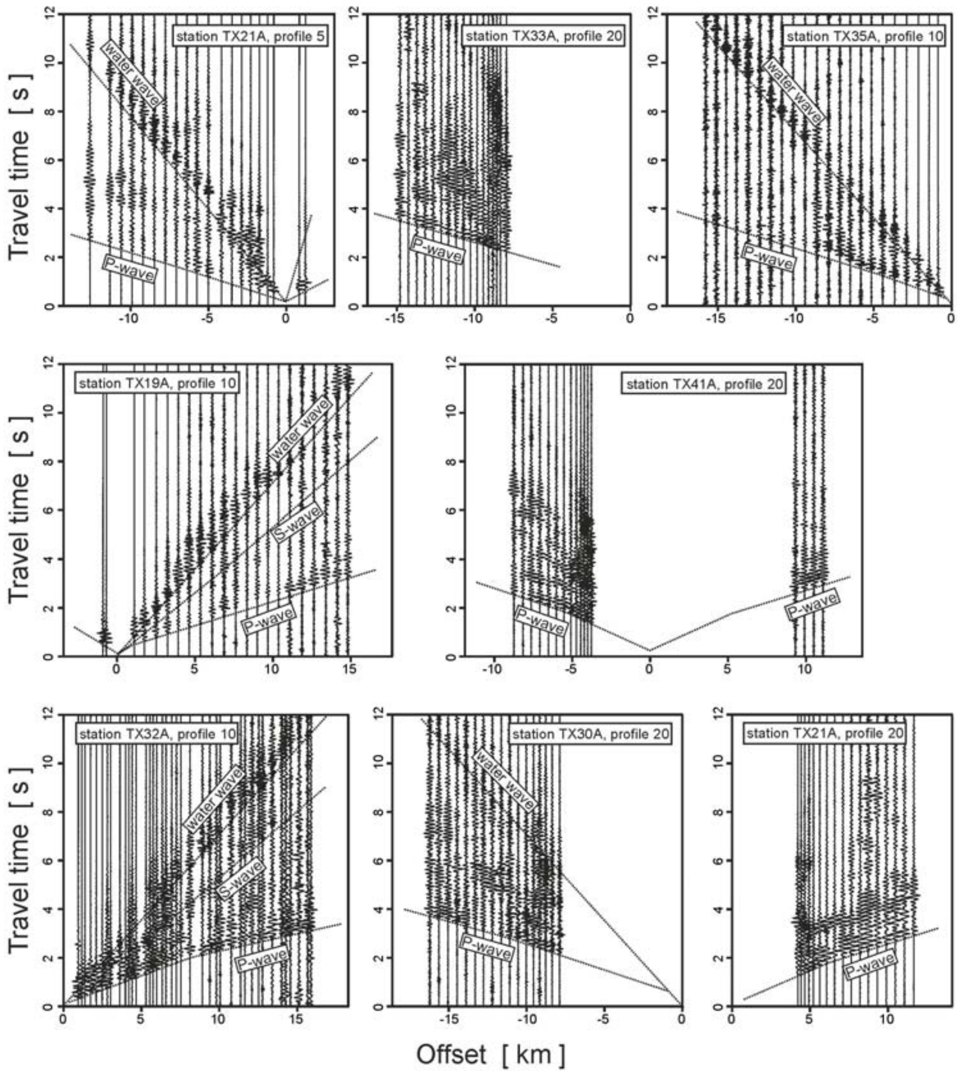

Fig. 4. An example of trace normalized, vertical component seismic record sections from experiment in the Admiralty Bay. The P waves are clearly observed for all offsets, most of the sections contains also water waves. In some sections S waves were recorded.

ate the bathymetric map of the study area (Fig. 3) by simple linear interpolation. Examples of the recorded seismic wave-field are presented in Fig. 4. The strong P-wave energy is observed at all stations even at the maximum distance of 17 km. In some of the record sections we can also distinguish strong S-waves. Relatively large distances between the shot points make it hard to correlate reflected waves because of the complicated system of multiples and converted waves. We decided to use the first arrivals of the Pg waves for tomography since this phase was

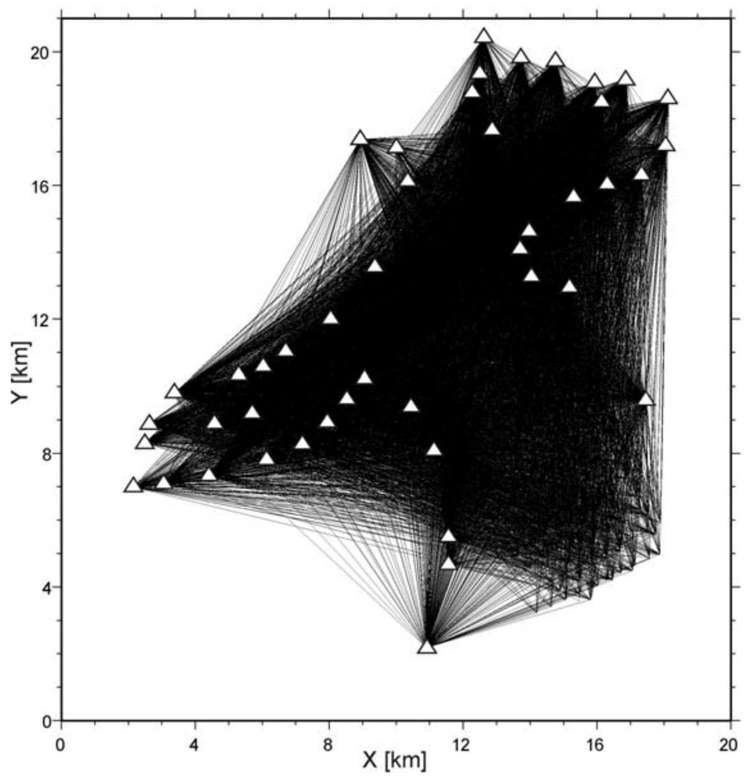

Fig. 5. The ray distribution of 11,341 manually picked and verified travel times of Pg waves used in interpretation. The white triangles mark the position of the stations. The area of the Admiralty Bay is well covered. Good coverage is also observed for the part of the land areas of Warszawa and Kraków blocks.

easily and indisputably observed for all stations and was characterised by a good signal-to-noise ratio. All traces were manually correlated, picked and verified using ZPLOT software (Zelt 1994). The total number of 11,341 ray paths cover the entire area (Fig. 5) and the full first arrival travel times data set is presented in Fig. 6. Observed scattering of the travel times (*ca* 1 s) for the same distance is caused mostly by varying water depth beneath the shots (Fig. 6 top) but it also suggests differences in the uppermost crustal structure. This is especially visible after removing the water-layer effect (Fig. 6 bottom).

Modelling of the upper crustal structure

Dimensions of the modelling area were 20 × 21 × 4 km (x, y, z) and geographical area is bounded by longitude 58.66–58.27 W and by latitude 62.25–62.06 S. Topography was not included because all stations were located at the coast only a

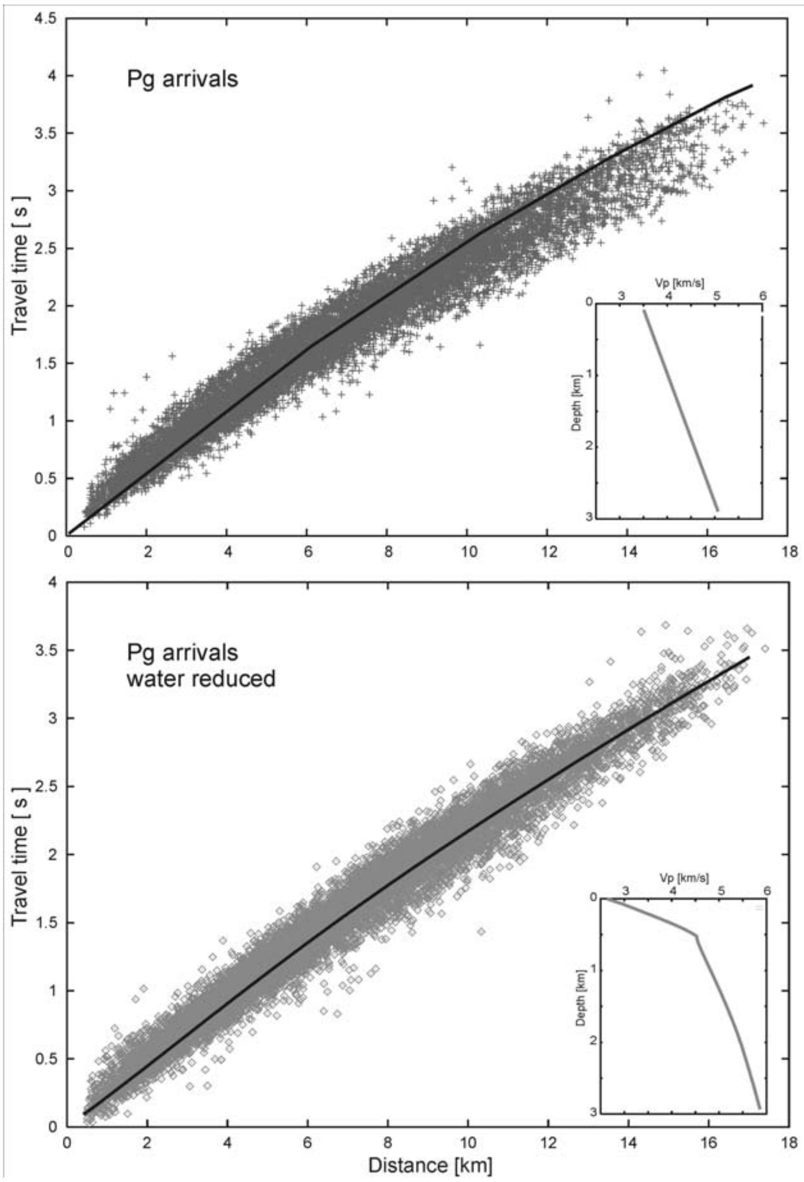

Fig. 6. All travel times plotted against the distance (top) shows significant scattering up to 1 second at the distance of 10 km. This suggests significant difference in the water column thickness beneath the shot points. The maximum distance between the shot and receiver was about 18 km. Travel times after the effect of the water layer was removed (bottom) are less scattered. 1D starting models for the inversions are presented in the inserts. Black lines present calculated starting model travel times.

few meters above the sea level and all shots were a few meters below the sea level. Modelling of the P-wave velocity structure of the uppermost crust was done using two methods of first arrival travel time tomography: “smooth“ tomography (IBP) and tomography with layers (JIVE3D). Results of the modelling are presented in Figs. 7–10.

“Smooth” tomography (IBP). — We started our tomographic modelling with the Iterative Back Projection code (IBP) of Hole (1992). It allows to create a minimum structure, “smooth” velocity model based on first arrival travel times. In this application the whole model is described by velocity values in a regular grid. It is not possible to include the water layer but it is still possible to correct travel times and remove the effect of variable water depth. For each shot, the travel time through the known thickness of the water layer was calculated (sea water Vp taken as 1.48 km/s) and all travel times from that shot were corrected by subtracting this time. In this way, shots are treated as they were located at the sea bottom and thus the travel time variations reflect only the differences in the crustal structure. A cubic cell with 0.2 km length was used to parametrize the model. To find the best starting model, the corrected travel times were used to calculate an initial 1D velocity model (see Fig. 6 bottom). This assures that the starting model is close to the real structure, which reduces the non-linearity posed by tomographic inversion. We performed the inversion in following steps: (1) limitation of maximum offset (up to 4, 8, 12 km, no limit) and (2) several sub-inversions with different smoothing factors 32×32×8 and 16×16×4 cells in x, y and z direction respectively. That assures stability and allows to model the shallow structures first. Together the inversion went through 16 iterations (2 steps for each parameter set). Obtained results are presented as the depth slices in Fig. 7 (left). In order to present only reliable results all cells that were not covered by rays are masked. We observe significant difference in the velocities between NW and SE part of the study area. It is especially visible at 400 m depth, where over 1 km/s differences in P-wave velocity exists between units divided by the Ezcurra Fault. When interpreting results of the “smooth” tomography based on first arrivals only, one should bear in mind that the sharp velocity contrast (*e.g.* faults, intrusions) can not be modelled. Such a structures are usually recognised as zones of higher velocity gradient. Modelled strong velocity gradient in the Ezcurra Inlet correlates well with the SW-NE Ezcurra Fault from surface mapping. Similar gradient zone in the Martel Inlet can be interpreted as the NE part of the Ezcurra Fault. In general, the study area can be divided into two units with: Vp > 4 km/s at Z = 200 m and Vp > 5 km/s at Z = 400 m in NW part (Barton Horst) and with Vp *ca* 3.6 km/s at Z = 200m and Vp *ca* 4.3 km/s at Z = 400 m in the SE part (Warszawa block). A strong gradient zone in SW-NE direction with relatively smaller gradient in the middle part separates these regions. The vertical slices presented in Fig. 8 show a strong gradient zone interpreted as the Ezcurra Fault in the Ezcurra Inlet (slice x = 5 km). This gradient disappears eastwards (slices x = 10 and 15 km). The contrast in Vp corresponding to the Ezcurra Fault is also visible at the slice y = 10 km. For y = 15 km this contrast is weaker and observed at the edge of the area covered by rays.

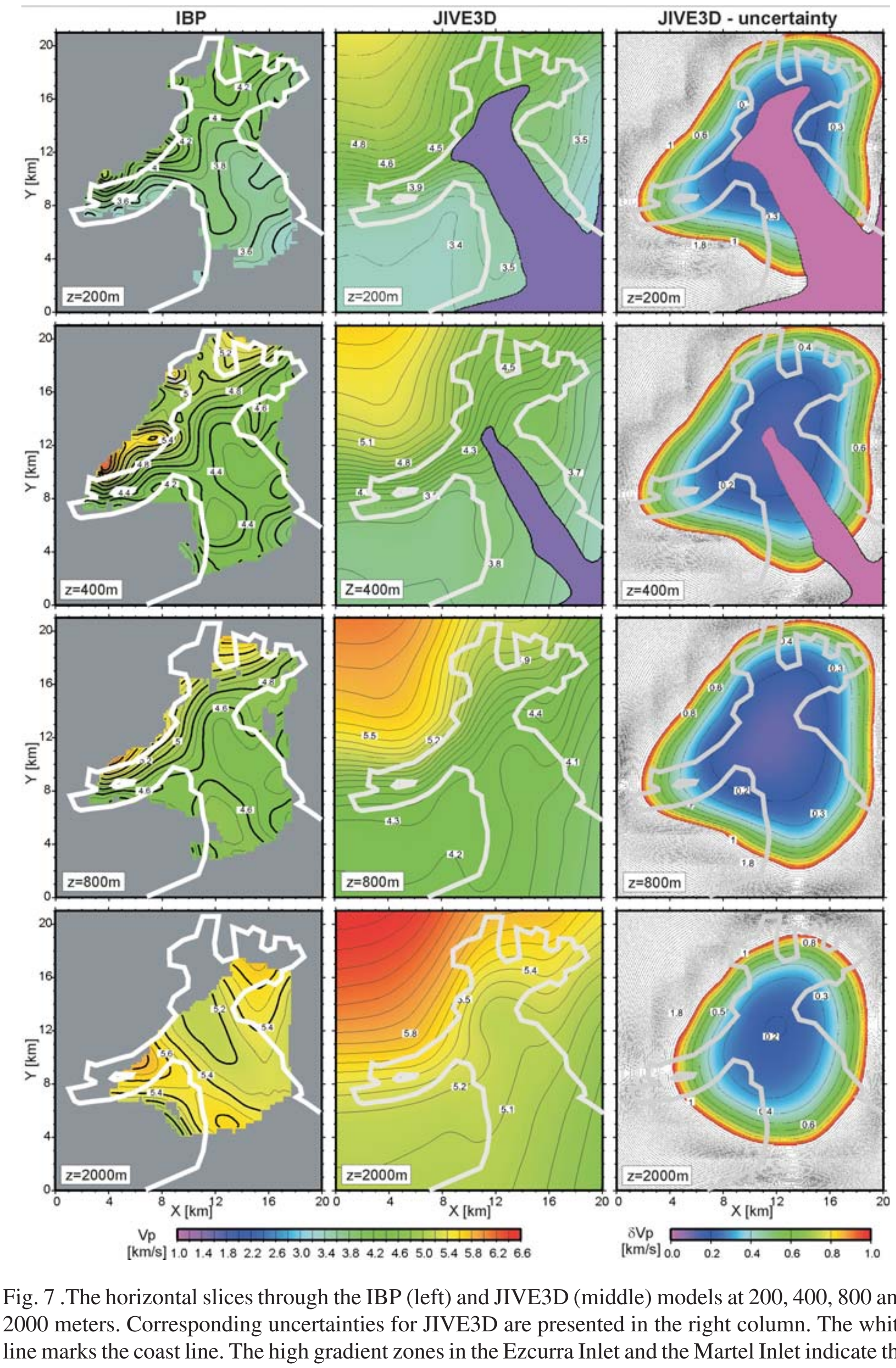

Fig. 7 .The horizontal slices through the IBP (left) and JIVE3D (middle) models at 200, 400, 800 and 2000 meters. Corresponding uncertainties for JIVE3D are presented in the right column. The white line marks the coast line. The high gradient zones in the Ezcurra Inlet and the Martel Inlet indicate the faults. Significant difference for the shallow structures in the velocities are visible between northern part (Barton Horst) with velocities about 4.5 km/s and the southern blocks with 3.5 km/s.

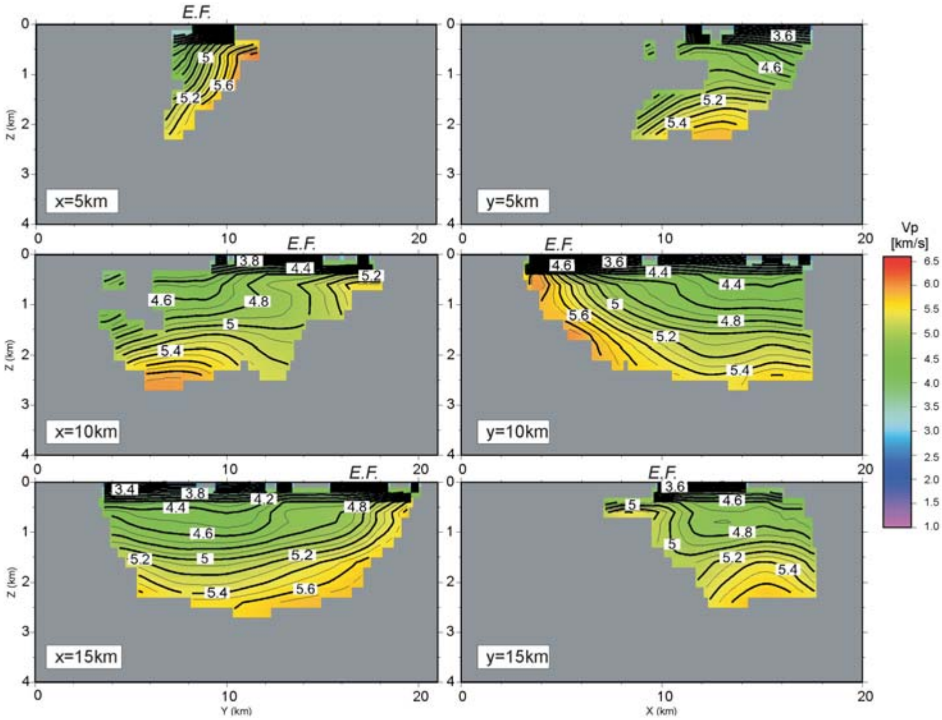

Fig. 8. The vertical slices through the IBP model at x equal 5, 10 and 15 km and y equal 5, 10 and 15 km. The velocities are presented in the areas with the ray coverage reaching to the depth of 2 km. A high gradient zone visible at x = 5 km is weakening northward. At y slices the strongest gradient is visible for y = 10 km. *E.F.* – Ezcurra Fault.

Tomography with bathymetry (JIVE3D). — We tested also another implementation of seismic tomography – JIVE3D code (Hobro, 1999). It allows to build velocity models with interfaces and separate velocity grids in each layer using not only first arrival travel times but also secondary phases including reflected waves. However, similarly to the IBP method, we used only first arrivals. The only difference was that we explicitly included bathymetry as one of the model interfaces. Because JIVE3D uses different model parameterization and interpolation (cubic B-splines) in comparison to IBP method, the obtained velocity fields are smoother. Velocity model was parameterized on the 1×1×0.5 km grid and 1×1 km grid was used for defining bathymetry. The inversion procedure was divided into 4 iterations with different smoothing factors and further subdivided into 6 iteration (24 steps in total). JIVE3D algorithm allows to obtain the *a posteriori* covariance matrix of the tomographic inversion and hence produces a measure of the model parameter uncertainty. This is a good way of estimating the relative reliability of the model parameters. The obtained results are presented as slices through the model with corresponding slices through the uncertainty field (Figs. 7, 9, 10). The depth slices (Fig. 7 middle) shows similar results as the IBP inversion. In the Ezcurra In-

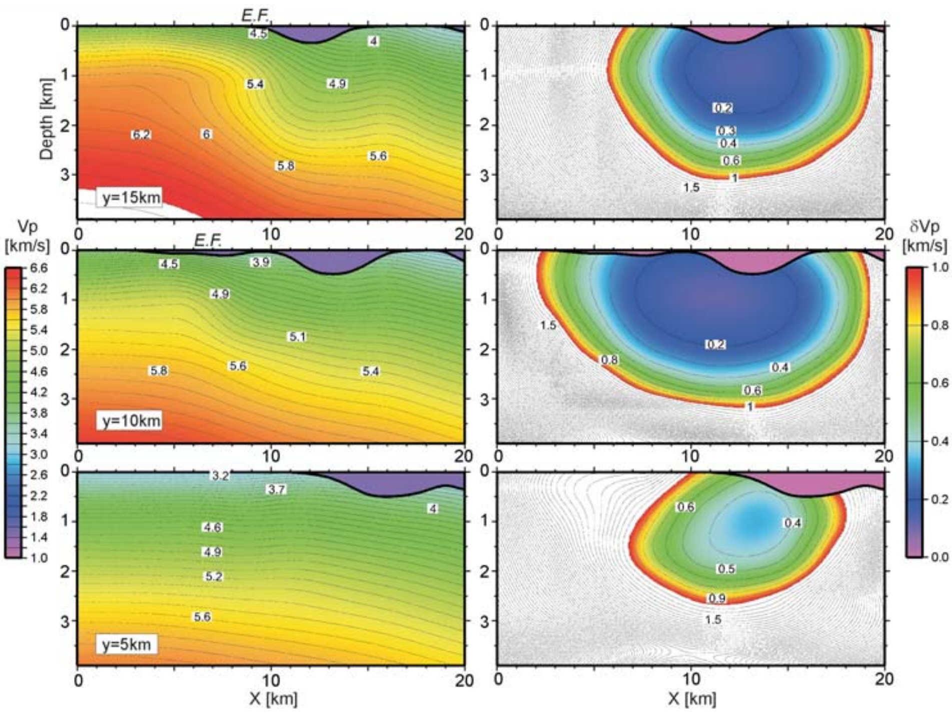

Fig. 9. The vertical slices through the JIVE3D model at coordinate y equal 5, 10 and 15 km with corresponding uncertainty estimation. The localization of the fault is easily visible as a rapid change in the isolines. It is more significant at y = 15 km and disappears southward. The fault can be traced to the depth of about 2 km. For deeper areas the uncertainty is too high for this model to be reliable. *E.F.* – Ezcurra Fault.

let and the Martel Inlet strong gradient are visible. This strong gradient can be traced as a continuous line up to the depth of 800 m, but it is not so significant in the middle part for deeper areas. The velocities in the NW block are much higher (Vp = 4.5 km/s at the depth of 200 m) in the area which is reliable according to the uncertainty values, while in the SE block velocity reaches only 3.4 km/s. In the deeper slices strong differences in the velocity can be also observed. Looking at the vertical slices (Fig. 9) we can clearly see position of the Ezcurra Fault, which is visible as a rapid change in the shape of isolines. It is more significant at y = 15 km and disappears southward. Taking into account the uncertainty values, we can trace the fault to the depth of 2 km. At the second set of slices (Fig. 10) this fault is visible at x = 5 km disappearing eastward.

Conclusions

The 2007 experiment allowed successful imaging of the shallow crustal structure in the Admiralty Bay. Good data quality, especially the first arrivals of Pg

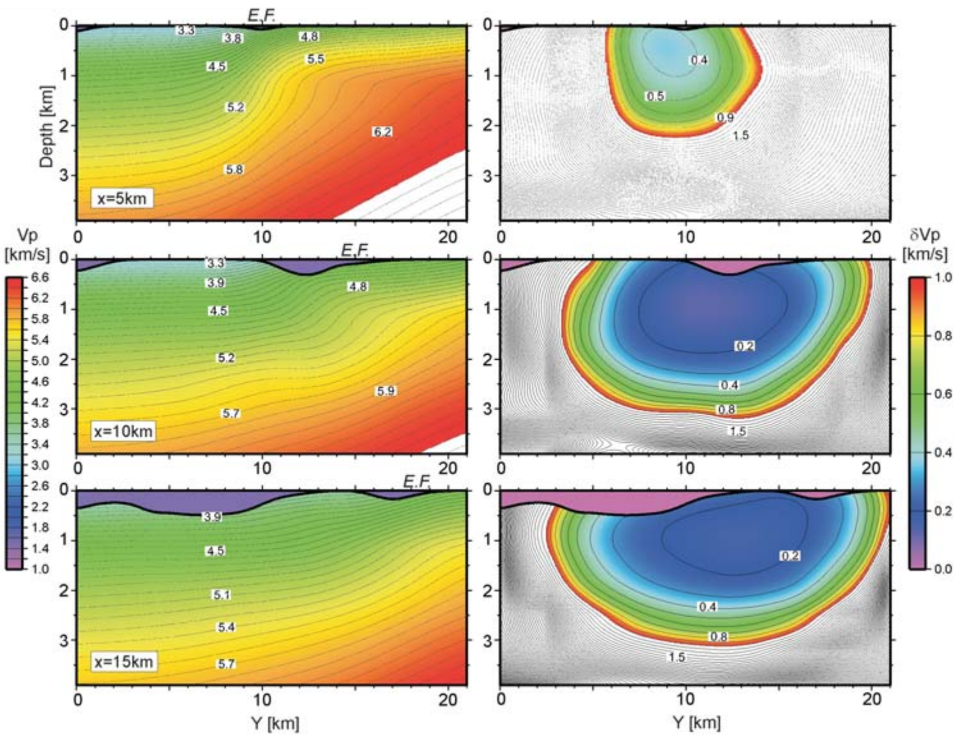

Fig. 10. The vertical slices through the JIVE3D model at x equal 5, 10 and 15 km with corresponding uncertainty estimation. The fault is easily visible at x = 5 km and disappears eastward. *E.F.* – Ezcurra Fault.

waves allowed us to perform 3D tomographic inversion. Our interpretation is presented in Fig. 11. We were able to track the Ezcurra Fault from the Ezcurra Inlet down to the depth of 2 km in the SW part of our area up to the Martel Inlet in the NE part (marked with thick black lines). We can not confirm the existence of this fault below 1 km depth in the middle part of the area and the stronger gradient is visible to the north from previously postulated location. Because of the insufficient ray coverage in the Kraków block (land area) we could not verify the existence of the Mackellar Fault. By comparing the velocities we can easily distinguish the Barton Horst with higher velocities of 4.5 km/s in the shallow structures from Warszawa and Krakow blocks with velocities of 3.5 km/s, which suggests that the Barton Horst was uplifted. Additionally the isoline of 4 km/s was presented to show an estimated edge of the Barton Horst, that is marked with gray fill. It was not possible to observe a difference in the structure of Warszawa and Kraków blocks. There were no significant differences between parts of Barton Horst: Cordozo Cove, Dufayel Island and Martel Inlet group. Supposed sharp boundaries or faults between them were to small comparing too the resolution of our data. Nevertheless, velocities observed in the western part of Barton Horst (Cordozo Cove and

Fig. 11. Schematic interpretation with marked localization of confirmed faults (thick black lines). The middle part of the Ezcurra Fault was not confirmed, as well as no proof for the Mackellar Fault near the Kraków block was found. Significant difference in the velocities on both sides of the fault system indicate the uplift of the Barton Horst. The 4.0 km/s isoline marks the edge of the Barton Horst. The yellow lines mark the positions of the vertical slices. Other markers as in Fig. 2.

Dufayel Island) are higher that those in eastern part (Keller Peninsula and Martel Inlet) on all verified depths.

Additionally, we managed to effectively use the Reftek 125 "Texan" stations with external battery packs in the antarctic conditions. For particular profiles it would be possible to perform more detailed ray tracing analysis using also recorded S-waves and other P-waves.

Acknowledgements. — This experiment was a part of the project PBZ-KBN-108/P04/2004 – a preparatory Polish scientific programme before the International Polar Year. We would like to thank the Captain and the crew of the MS *Polar Pioneer*. For map preparation and coordinate calculations we used GMT software (Wessel and Smith 1998). We thank Dr Michael Behm and Dr Timo Tiira for carefully reviewing the manuscript.

References

ACOSTA J., HERRANZ P., SANZ J.L. and UCHUPI E. 1992. Antarctic Continental Margin: Geologica Image of the Bransfield Trough, An Incipient Ocean Basin. *In*: C.W. Poag and P.C. de Graciansky (eds) *Geologic Evolution of the Atlantic Continental Rises*. Van Nostrand Reinhold, New York: 49–61.

BARKER P.F. 1982. The Cenozoic subduction history of the Pacific margin of the Antarctic Peninsula: ridge crest – trench interactions. *Journal of Geological Society, London* 139: 787–802.

BARKER P.F. and DALZIEL I.W.D. 1983. Progress in geodynamics in the Scotia Arc region. *In*: R. Cabré (ed.) *Geodynamics of the Eastern Pacific Region, Caribbean and Scotia Arcs*. Geodynamics Series American Geophysical Union Series, Washington DC 9: 137–170.

BIRKENMAJER K. 1989. A guide to Tertiary geochronology of King George Island, West Antarctica. *Polish Polar Research* 10: 555–579.

BIRKENMAJER K. 2003. Admiralty Bay, King George Island (South Shetland Islands, West Antarctica): a geological monograph. *In*: K. Birkenmajer (ed.) Geological results of the Polish Antarctic expeditions. *Studia Geologica Polonica* 120: 5–73.

BIRKENMAJER K. and KELLER R.A. 1990. Pleistocene age of the Melville Peak volcano, King George Island, West Antarctica, by K-Ar dating. *Bulletin of the Polish Academy, Earth Sciences* 38 (1–4): 17–24.

CHRISTESON G.L., BARKER D.H.N., AUSTIN J.A. JR. and DALZIEL I.W.D. 2003. Deep crustal structure of Bransfield Strait: Initiation of a back arc basin by rift reactivation and propagation. *Journal of Geophysical Research* 180, B10, 2492, doi: 10.1029/2003JB002468.

DALZIEL I.W.D. and ELLIOT D.H. 1973. The Scotia arc and Antarctic margin. *In*: A.E.M. Narin and F.G. Stehli (eds) *The ocean basins and margins (the South Atlantic)*. Plenum Press, New York and London: 171–246.

GONZÁLEZ-FERRÁN O. 1985. Volcanic and tectonic evolution of the northern Antarctic Peninsula – Late Cenozoic to Recent. *In*: E.S. Husebye, G.L. Johnson and Y. Kristoffersen (eds) Geophysics of the Polar Regions. *Tectonophysics* 114: 389–409.

GRAD M., GUTERCH A. and ŚRODA P. 1992. Upper crustal structure of Deception Island area, Bransfield Strait, West Antarctica. *Antarctic Science* 4: 469–476.

GRAD M., GUTERCH A. and JANIK T. 1993. Seismic structure of the lithosphere across the zone of subducted Drake plate under the Antarctic plate, West Antarctica. *Geophysical Journal International* 115: 586–600.

GRAD M., GUTERCH A., JANIK T. and ŚRODA P. 2002. Seismic characteristic of the crust in the transition zone from the Pacific Ocean to the northern Antarctic Peninsula, West Antarctica. *In*: J.A. Gamble, D.N.B. Skinner and S. Henrys (eds) *Antarctica at the close of a millennium*. Royal Society of New Zealand 35: 493–498.

GUTERCH A., GRAD M., JANIK T. and ŚRODA P. 1998. Polish Geodynamic Expeditions – seismic structure of West Antarctica. *Polish Polar Research* 19 (1–2): 113–129.

GUTERCH A., GRAD M., JANIK T., PERCHUĆ E. and PAJCHEL J. 1985. Seismic studies of the crustal structure in West Antarctica 1979–1980 – preliminary results. *In:* E.S. Husebye, G.L. Johnson, Y. Kristoffersoen (eds) Geophysics of the Polar Regions. *Tectonophysics* 114: 411–429.

HOBRO J.W.D. 1999. Three-dimensional tomographic inversion of combined reflection and refraction seismic travel-time data. Ph.D. Thesis. Department of Earth Sciences, University Cambridge: 240 pp.

HOLE J.R. 1992. Non-linear high resolution three-dimensional seismic travel time tomography. *Journal of Geophysical Research* 97: 6553–6562.

JANIK T., ŚRODA P., GRAD M. and GUTERCH A. 2003. Moho Depth along the Antarctic Peninsula and Crustal Structure across the Landward Projection of the Hero Fracture Zone. *In*: D.K. Fütterer, D. Demaske, G. Kleinschmidt, H. Miller and F. Tessensohn (eds) *Antarctica Contributions to Global Earth Sciences*. Proceedings of the IX International Symposium of Antarctic Earth Sciences, Potsdam: 229–236.

PELAYO A.M. and WIENS D.A. 1989. Seismotectonics and relative plate motions in the Scotia Sea region. *Journal of Geophysical Research* 94 (B6): 7293–7320.

ŚRODA P. 1991. Determination of the crustal structure in the region of Deception Island (West Antarctica) using one- and two-dimensional seismic modelling. M.Sc. Thesis. Institute of Geophysics, University of Warsaw: 46 pp. (in Polish).

ŚRODA P. 2002. Three-dimensional seismic modelling of the crustal structure between the South Pacific and the Antarctic Peninsula. *In*: J.A. Gamble, D.N.B. Skinner and S. Henrys (eds) *Antarctica at the close of a millennium*. Royal Society of New Zealand 35: 555–561.

ŚRODA P., GRAD M. and GUTERCH A. 1997. Seismic Models of the Earth's Crustal Structure between the South Pacific and the Antarctic Peninsula. *In*: C.A. Ricci (ed.) *The Antarctic Region: Geological Evolution and Processes*. Terra Antarctica Publications, Siena: 685–689.

TAYLOR F.W., BEVIS M.G., DALZIEL I.W.D., SMALLEY R. JR., FROHLICH C., KENDRICK E., FOSTER J., PHILLIPS D. and GUDIPATI K. 2008. Kinematics and segmentation of the South Shetland Islands-Bransfield basin system, northern Antarctic Peninsula. *Geochemistry, Geophysics and Geosystems* 9, Q04035, doi:10.1029/2007GC001873

WESSEL P. and SMITH W.H.F. 1998. New, improved version of the Generic Mapping Tools released, EOS. *Transactions American Geophysical Union* 79: 579.

ZELT C.A. 1994. ZPLOT – an interactive plotting and picking program for seismic data. Bullard Labs, University of Cambridge, Cambridge UK.

Received 3 July 2008
Accepted 28 August 2008